© 2014. Published by The Company of Biologists Ltd | The Journal of Experimental Biology (2014) 217, 3045-3056 doi:10.1242/jeb.101568

RESEARCH ARTICLE

Encoding properties of the mechanosensory neurons in the Johnston's organ of the hawk moth, *Manduca sexta*

Alexandre Dieudonné[1,*], Thomas L. Daniel[1] and Sanjay P. Sane[2,*]

ABSTRACT

Antennal mechanosensors play a key role in control and stability of insect flight. In addition to the well-established role of antennae as airflow detectors, recent studies have indicated that the sensing of antennal vibrations by Johnston's organs also provides a mechanosensory feedback relevant for flight stabilization. However, few studies have addressed how the individual units, or scolopidia, of the Johnston's organs encode these antennal vibrations and communicate it to the brain. Here, we characterize the encoding properties of individual scolopidia from the Johnston's organs in the hawk moth, *Manduca sexta*, through intracellular neurophysiological recordings from axons of the scolopidial neurons. We stimulated the flagellum–pedicel joint using a custom setup that delivered mechanical stimuli of various (step, sinusoidal, frequency and amplitude sweeps) waveforms. Single units of the Johnston's organs typically displayed phaso-tonic responses to step stimuli with short (3–5 ms) latencies. Their phase-locked response to sinusoidal stimuli in the 0.1–100 Hz frequency range showed high fidelity (vector strengths>0.9). The neurons were able to encode different phases of the stimulus motion and were also extremely sensitive to small amplitude (<0.05 deg) deflections with some indication of directional tuning. In many cases, the firing frequency of the neurons varied linearly as a function of the stimulus frequency at wingbeat and double wingbeat frequencies, which may be relevant to their role in flight stabilization. Iontophoretic fills of these neurons with fluorescent dyes showed that they all projected in the antennal mechanosensory and motor center (AMMC) area of the brain. Taken together, these results showcase the speed and high sensitivity of scolopidia of the Johnston's organs, and hence their ability to encode fine antennal vibrations.

KEY WORDS: Lepidoptera, Antennae, Mechanosensors, Johnston's organ, Scolopidia, Electrophysiology, Flight

INTRODUCTION

Flying insects rely on both visual and mechanosensory information during fast aerial maneuvers. Although combined input from both of these modalities is necessary for flight, each provides feedback at different latencies. Owing to its reliance on second-messenger systems for photo-transduction (e.g. Hardie and Raghu, 2001), visual feedback tends to be slower than mechanosensation. In low light, visual latencies may be further slowed by the time required for image formation (Warrant, 2006; Theobald et al., 2010). Models of flight control in moths suggest that visual delays combined with inherent instability associated with flapping flight present significant challenges for flying insects (Hedrick and Daniel, 2006). Hence, vision alone may be insufficient to mediate flight stability and control in the absence of mechanosensory feedback (Sane et al., 2007).

In Diptera, a pair of organs called halteres provides the mechanosensory feedback essential for maintaining equilibrium during flight. During aerial maneuvers, halteres maintain balance by transducing information about Coriolis torques resulting from body rotations (Pringle, 1948; Hengstenberg, 1988; Nalbach, 1993; Fayyazuddin and Dickinson, 1996; Frye and Dickinson, 2004). These forces, calculated by the cross-product of the angular velocity of the body and linear velocity of vibrating halteres (Nalbach, 1993) are thought to cause lateral displacements in haltere stroke plane, which are detected by fields of campaniform sensilla at the base of each haltere. The haltere afferents make monosynaptic connections with the motor neurons of wing steering muscles, thus providing rapid sensory feedback for course corrections (Fayyazuddin and Dickinson, 1996; Fox et al., 2008; Fox et al., 2010). Indeed, the role of halteres in detecting body rotations is a key feature of flight control in Diptera.

In hawk moths, antennal mechanosensors play a crucial role in flight control (Sane et al., 2007). The basal antennal mechanosensory apparatus requires proper mechanical loading for flight stability. During flight, moth antennae vibrate at wingbeat frequency and hence experience Coriolis torques at the base of their antennae during aerial turns at frequencies that are approximately twice the wingbeat frequency [see figs S2 and S4 of Sane et al. (Sane et al., 2007)]. Because a subset of scolopidia of the Johnston's organ are tuned to the frequency range of Coriolis-based strains, antennal mechanosensors have been hypothesized to serve a function similar to that of Dipteran halteres. Moths with unloaded Johnston's organs can not control their flight trajectories, but regain control when flagella are reattached (Sane et al., 2007). In tethered and freely flying hawk moths, antennal mechanosensors influence active flexing of the abdomen, which may in turn influence flight stability (Hinterwirth and Daniel, 2010; Hinterwirth et al., 2012).

In addition to their role in stabilizing flight, Johnston's organs also serve other functions in different insects. In flies, they are thought to sense changes in airflow via detection of antennal deflections, enabling insects to control their flight velocity and orientation in the yaw axis (Budick et al., 2007; Mamiya et al., 2011). Two recent studies in *Drosophila* have established that Johnston's organs contain a combination of scolopidial units, some are tuned to low frequency stimuli, such as gravity or air flow, whereas others are tuned to high-frequency signals, such as auditory signals associated with the wing vibration during mating (Kamikouchi et al., 2009; Yorozu et al., 2009). Similarly, small tortoiseshell butterflies, *Aglais urticae*, are also thought to use their antennae for sensing relative air flow (Niehaus and Gewecke, 1978; Gewecke and Niehaus, 1981a; Gewecke and Niehaus, 1981b). These studies argue for a multi-functional role of antennal mechanosensors during flight.

[1]Department of Biology, University of Washington, Seattle, WA 98195, USA.
[2]National Centre for Biological Sciences, Tata Institute of Fundamental Research, Bangalore 560065, India.

*Authors for correspondence (alexdieu@uw.edu; sane@ncbs.res.in)

Received 19 December 2013; Accepted 10 June 2014

The Journal of Experimental Biology (2014) doi:10.1242/jeb.101568

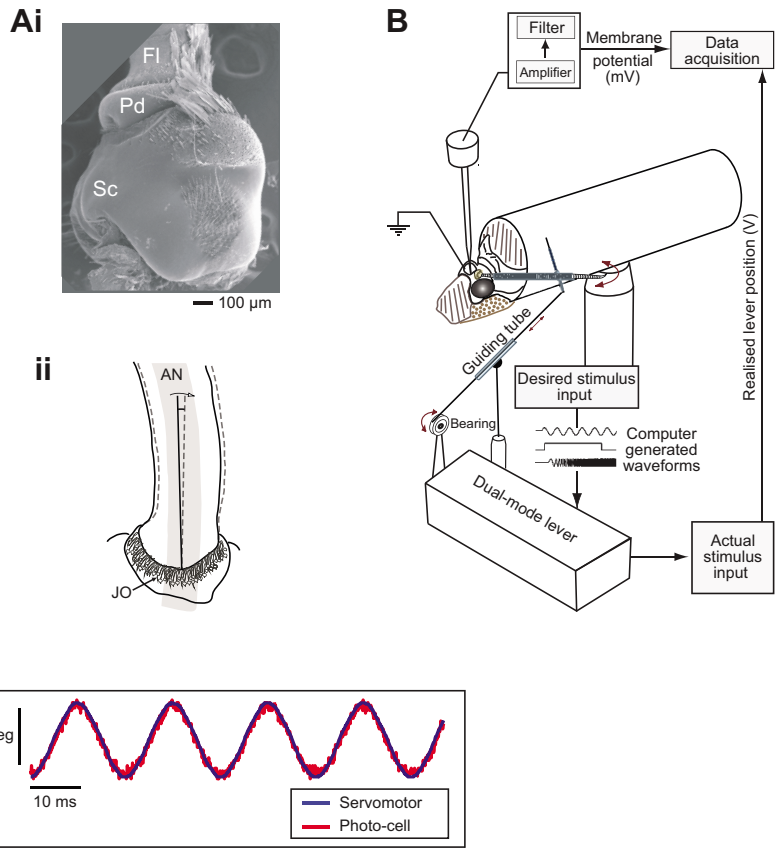

Fig. 1. Experimental set-up for intracellular recordings of the scolopidial responses to antennal vibrations. (A) Scanning electron micrograph (i) of the base of *M. sexta* antenna, including the basal scape (Sc) segment, medial pedicel (Pd) segment and a distal multi-annular flagellum (Fl). (ii) Illustration adapted from Vande Berg (Vande Berg, 1971) of the base of the antennal apparatus with illustrations of the Johnston's organ (JO) and the antennal nerve (AN). The maximum deflection of the flagellum–pedicel passive joint during experiments ranged between 1.5 and 3°. The scape and pedicel were immobilized with a mixture of beeswax–rosin. (B) The set-up for intracellular electrophysiological recordings from the scolopidial neurons in the antennal Johnston's organ. An adult *M. sexta* was mounted dorsal side-up in a plastic tube. A mechanical servomotor was driven by pre-programmed waveforms and moved the antenna via an attached custom-built lever system. The actual motion of the lever arm was recorded as the stimulus signal for data analysis. The dorsal cuticle of the head capsule was removed to record from scolopidial neuron axons in the antennal nerve using sharp micropipette electrodes. (C) Comparison between the output signal of the servomotor (blue) and the motion of the flagellum measured using a photodiode system (red). The stimulus shown is a sinusoidal wave at 50 Hz.

How do the circuitry and encoding properties of individual scolopidial units of Johnston's organs relate to its overall function as a mechanosensory organ? Here, we address this question by describing the encoding characteristics of individual scolopidia in the Johnston's organ of the hawk moth, *Manduca sexta* (Linnaeus 1763). We provided the flagellar–pedicellar joint of the antenna with diverse mechanical stimuli while recording intracellularly from axons of individual scolopia to determine their frequency, amplitude and directional tuning. The scolopidial cell body locations and projection patterns were identified by iontophoretically staining them with fluorescent dyes. The data presented here provide insights into mechanosensory encoding properties of individual neurons in the Johnston's organ.

RESULTS

We recorded from antennal scolopidial neurons in *M. sexta* individuals (96 neurons; 29 male and female moths) that were stimulated by step, sinusoidal, sinusoidal frequency-sweep and sinusoidal amplitude-sweep mechanical stimuli (Materials and methods; Fig. 1A–C). Most neurons showed phase-locked spiking to sinusoidal stimuli in the 0–100 Hz range, typically responding with phaso-tonic firing patterns to step stimuli (5–300 s duration) with latencies on the order of ~3 ms (Table 1). We successfully filled a subset of these cells (N=43), which were all scolopidial units of the Johnston's organ. The neurons were sensitive to antennal movements as small as 0.05–0.02 deg.

Anatomy of the scolopidial neurons

Of 96 recorded neurons, we labeled 43 cells with either Lucifer Yellow (LY; 27 cells) or Alexa Fluor 568 (AF; 16 cells). Typically, each cell was marked with a distinct dye. In some cases, we filled more than one cell with the same dye. All filled neurons had the distinct morphology of scolopidial units of the Johnston's organ. Fig. 2A shows a montage of the dorsal view of a dissected *M. sexta* brain with intact antennal nerves and bases. Two scolopidial neurons from the left antenna were filled with Lucifer Yellow (Fig. 2A, magnified in images i–iii). Cell bodies of these neurons are embedded within the pedicel with a ciliary projection extending towards the flagellar base (Fig. 2Ai). Near the scapal base, the antennal nerve splits into two branches, and its cross-section shows two labeled axons from scolopidia within one of the branches (Fig. 2Aii). These neurons arborize ispilaterally in the antennal mechanosensory and motor center (AMMC) region of the deutocerebrum (Fig. 2Aiii). This organization was consistent in all

Table 1. Summary of the measured phase-locked responses of scolopidial neurons

Stimulus	N= (cells)	Phase locked	%	Poorly phase locked	%	Independent	%
Sin 0.1–5 Hz	64	52	81.2	6	9.4	6	9.4
Sin 1 –25 Hz	44	32	72.7	9	20.5	3	6.8
Sin 30–60 Hz	42	27	64.2	13	31.0	2	4.8
Sin 75–100 Hz	38	24	63.2	10	26.3	4	10.5

Phase-locked responses from a total of 96 scolopidial neurons were divided on the basis of their frequency range into four categories for sinusoidal (Sin) stimuli. Although each category spans a specific frequency range, some cells are common between these categories. The different firing behaviors (phase locked, partially phase locked and independent) are defined in the text and shown in Fig. 4A–C.

The Journal of Experimental Biology

The Journal of Experimental Biology (2014) doi:10.1242/jeb.101568

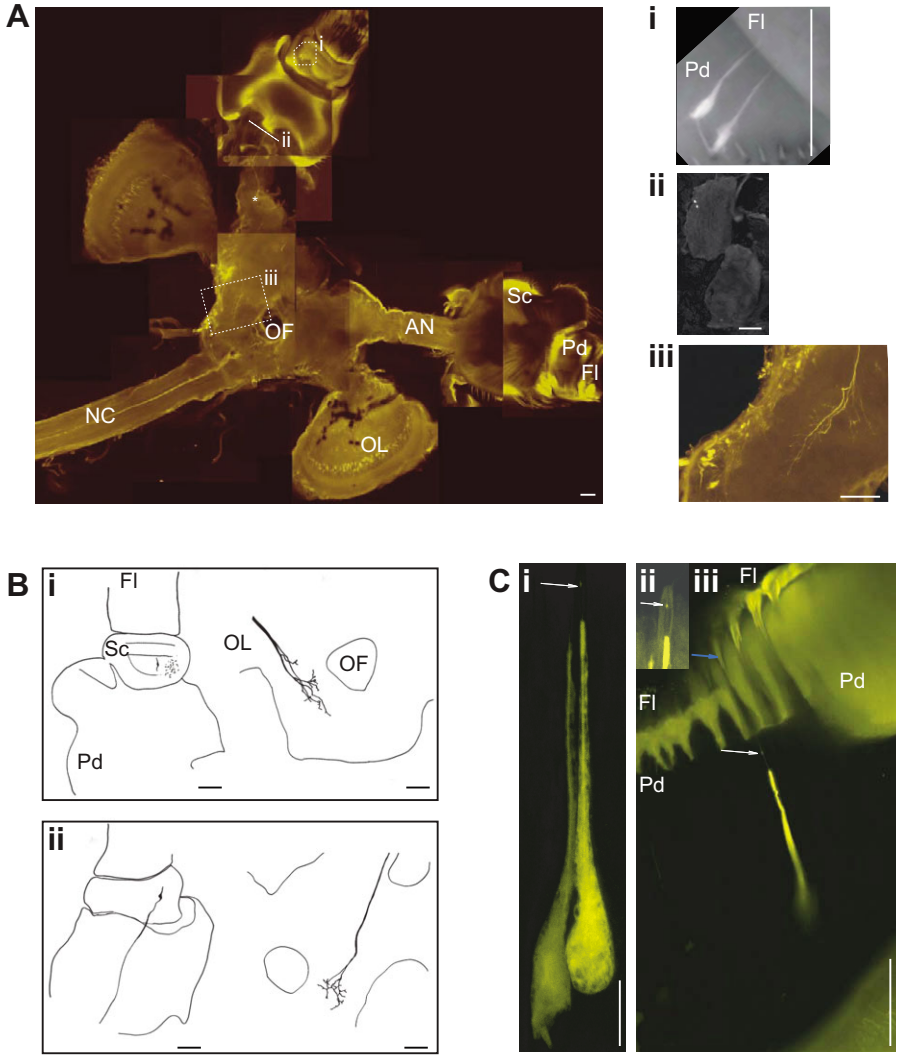

Fig. 2. Neuroanatomy of antennal scolopidial neurons. (A) Montage of the *M. sexta* nervous system, including both antennal nerves (AN) and intact bases with two scolopidial neurons filled with Lucifer Yellow. The three panels on the right display magnified sections from the montage designated by the dotted boxes and line. The scolopidial neurons have cell bodies located inside the pedicel (I, Pd) and their axons travel through one of the antennal nerve branches, evident as two spots in the antennal nerve cross section (ii). The two neurons arborize within the AMMC (iii). (B) Traced illustrations of the morphology of scolopidial neurons (soma and arborization locations) from two other individuals. Barring minor differences, this pattern of arborization was consistent in all 46 filled neurons. The shape of the arbor between the cells in the AMMC varies from cell to cell (e.g. i, elongated; ii, concentric). (C) High magnification (600×) images of two recorded scolopidial neuron cell bodies filled with Lucifer Yellow. One neuron extends a cilium with a ciliary dilation (i–iii, white arrow). The soma is located within the boundary of the pedicel, and an extension of the cilium attaches to the first annulus of the flagellum (Fl) (iii, blue arrow). NC, nerve cord; OF, esophageal foramen; OL, optic lobe; Sc, scape; *, recording site in the antennal nerve. See also supplementary material Movie 1 for a detailed view of the individual scolopidium filled with Lucifer Yellow during recordings. Scale bars: 100 µm (A,B); 10 µm (C).

filled neurons and was traced for two other scolopidial neurons from different moths (Fig. 2B). Subtle differences in projection patterns between cells reflected inter-cell or inter-individual variation. Some arborizations showed local ramifications (e.g. Fig. 2Bii), others extended in the caudal–rostral direction towards the subesophageal ganglia (Fig. 2Aiii, Fig. 2Bi). Our neuroanatomical method did not allow us to determine whether different groups of scolopidial neurons innervate specific zones of the AMMC, similar to those of the *Drosophila* brain (Kamikouchi et al., 2006; Kamikouchi et al., 2009; Yorozu et al., 2009).

An example of higher magnification (×600) fillet preparations revealed two scolopidial neurons (filled with Lucifer Yellow) with a cilium and its ciliary dilation (white arrow, Fig. 2Ci–iii; supplementary material Movie 1). A small extension, probably corresponding to one of three ciliary extensions described previously by Vande Berg (Vande Berg, 1971), connects the tip of the scolopidial cilium in the pedicel to the base of first annulus of flagellum (blue arrow, Fig. 2Ciii). We observed similar morphology in neural fills from other moths. Thus, the mode of mechanosensory transduction is likely to be similar in all scolopidia within the Johnston's organ.

Intracellular responses to mechanical stimuli

Step stimuli

We analyzed intracellular signals from 14 scolopidia in 10 moths to measure latency of the scolopidial response to step antennal movements. From the peri-stimulus time histograms (PSTH), constructed using the onset of action potentials to repeated step stimuli presentations, we computed the probability of spikes (P_{spike}) using the sampling rate resolution with bin sizes of 100 µs (red traces; Fig. 3A,B) by dividing the number of spikes within each bin by the total number of repeats across all cells and animals.

Most cells showed phaso-tonic responses to the onset (shaded area, left; Fig. 3A, top panel) of step motion. Immediately after step onset, many cells fired spikes with regular timing, perhaps owing to small ringing in the servo motor (slight bump in the blue trace between 3 and 10 ms; Fig. 3B). At the step offset (right shaded area; Fig. 3A), multiple cells also showed sharp responses. In a few cases, phasic responses were followed by a sharp decrease in firing rates (Fig. 3A, cells 1*, 4). This post-stimulus inhibitory response was observable in approximately 45% of the recorded neurons for any stimulus type. The other 55% of neurons responded to step offset with phaso-tonic activity similar to responses at step onset (Fig. 3A, cells 3*, 3**, 7, 9**, 10). The peak P_{spike} value of 0.104 and 0.133 (Fig. 3B, red curve, * and ** respectively) occurred ~3 ms after the step onset and offset, corresponding to the occurrence of the first post-stimulus spike across multiple trials in the raster plot. If we define the period between step onset (or offset) and the bin with highest firing probability as the latency of firing, scolopidial neurons responded with a latency of 3±0.7 ms (±s.d.; N=14 cells, 14 moths).

The Journal of Experimental Biology (2014) doi:10.1242/jeb.101568

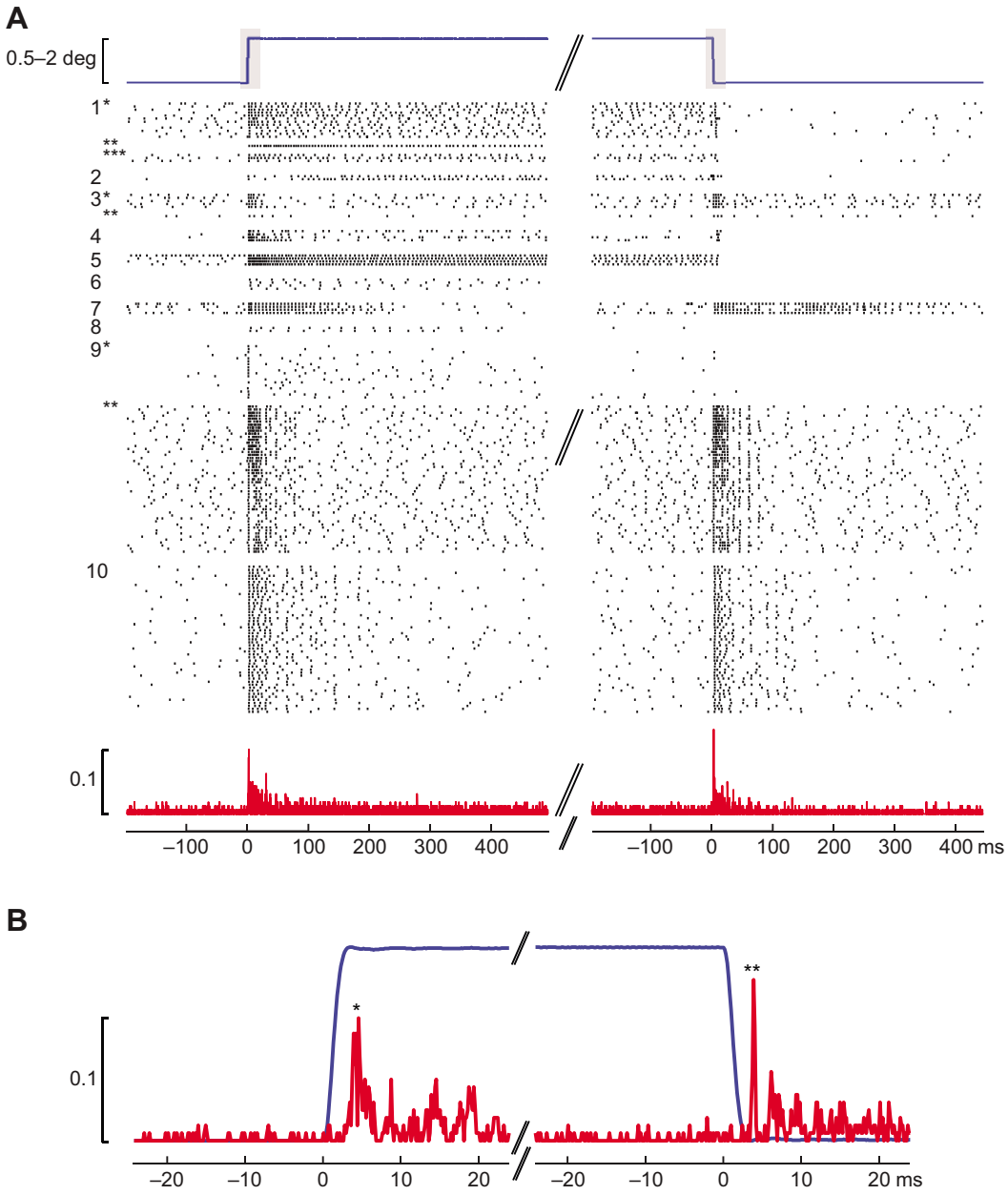

Fig. 3. Responses of scolopidial neurons to step motions of the antenna. (A) PSTH of 14 cells in 10 moths in response to a step stimulus (top panel, blue trace, regions of onset and offset of stimulus are indicated by the shaded areas). In the raster plot below the stimulus curve, each row represents a trial and the spiking occurrences as indicated by vertical black lines. Because the trials between insects were of varying durations (range 5–30 s), we display the recordings 200 ms pre- and 500 ms post-stimulus onset, and 200 ms pre- and 450 ms post-stimulus offset. Each insect is denoted by a number, and different cells for a given individual are denoted by stars. The number of recordings per trial ranges from 1 to 49. The red trace below the raster represents the firing probability computed using bins of 100 µs. The amplitude of the step (0.5–2 deg) was varied due to experimental variations. (B) Magnification of both the step and firing probability traces from A (shaded region). The peak probabilities of firing (*0.101 and **0.133) occur, respectively, ~3 ms after the onset and offset of the step motion.

Sinusoidal stimuli

We subjected scolopidial neurons to very low (0.1–5 Hz; N=64 neurons), low (10–25 Hz; N=44 neurons), medium (30–60 Hz; N=42 neurons) and high (75–100 Hz; N=38 neurons) frequency sinusoidal stimuli, sequentially. These included cells subjected to more than one type of stimulus (Table 1). A majority of the cells were phase locked [70%; vector strength (VS)>0.7] or partially phase locked (22%; 0.5<VS<0.7) to the stimulus. Thus, most cells (92%) effectively responded to frequencies between 0–100 Hz, covering the behavioral range of antennal vibrations under natural conditions (Sane et al., 2007). Fig. 4A shows a typical example of the phase-locked responses of a cell to varying frequency, sinusoidal stimuli of 1.5 deg amplitude applied to the passive pedicel–flagellum joint (upper traces, blue). The scolopidial neuron responded to low-frequency sinusoidal motion with a burst of spikes (lower traces, red) with precise phase locking, as represented by the shape of the Gaussian-convolved firing rate (GCFR; Fig. 4A, 0.2 Hz, 1 Hz, 5 Hz, middle traces, black). The firing rate co-varied with stimulus such that, as stimulus frequency increased, the cell fired fewer spikes per period of oscillation (Fig. 4A, compare 1 and 10 Hz). At the highest frequencies, the neuron fired single spikes per period (Fig. 4A, 100 Hz). For this

The Journal of Experimental Biology (2014) doi:10.1242/jeb.101568

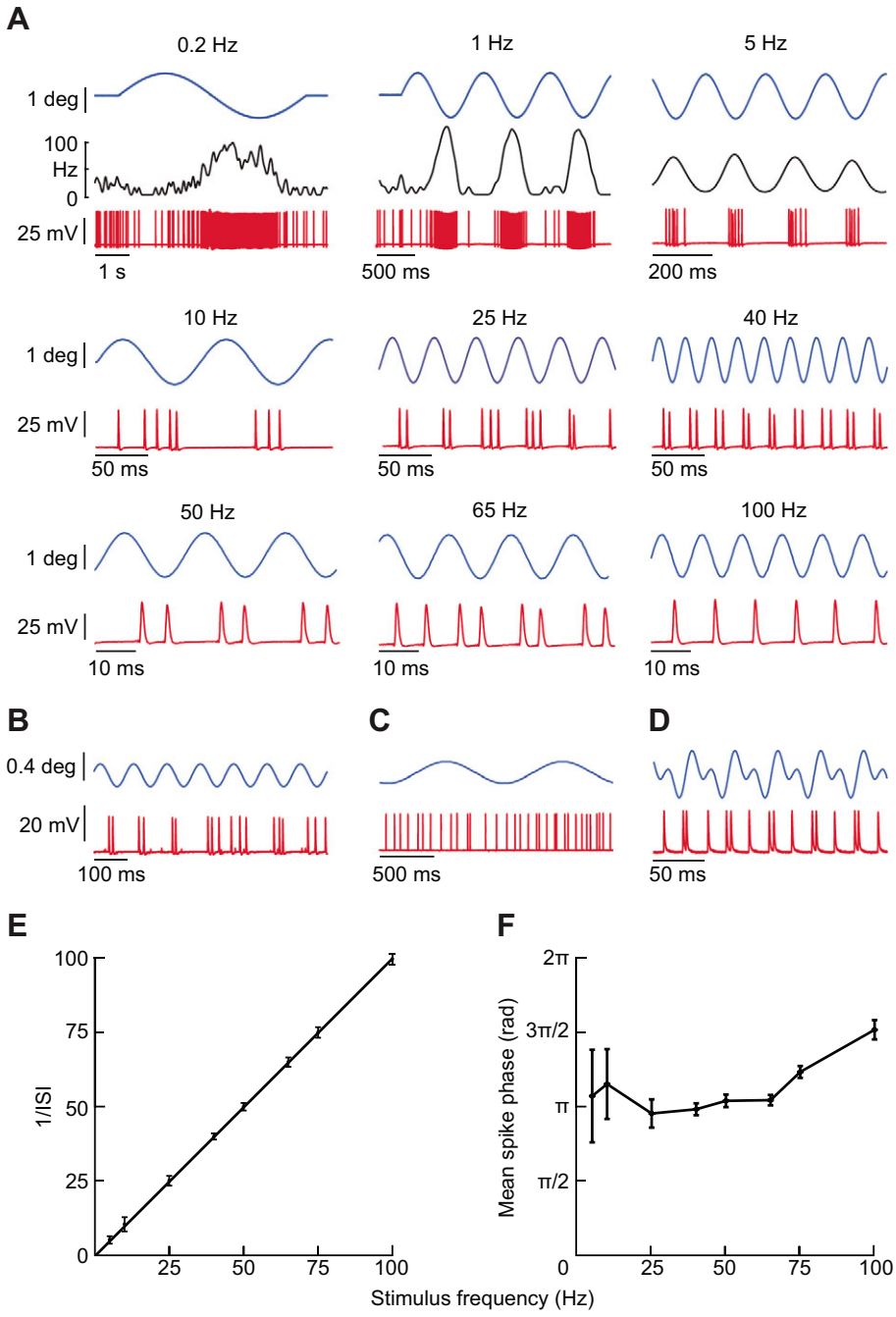

Fig. 4. Responses of scolopidial neurons to sinusoidal antennal motions. (A) Phase-locked response of a scolopidial neuron to sinusoidal frequency motion from 0.2–100 Hz. In each sub-figure, represented with its specific stimulus frequency, the top trace (blue) is the flagellum position, the middle trace shows the GCFR (black, only for the low frequencies 0.2, 1 and 5 Hz, first row) and the bottom trace (red) shows the membrane potential displaying the action potentials. (B) An example of a partially phase-locked scolopidial neuron to a 10 Hz sinusoidal motion (flagellum position, top trace, blue; membrane potential, bottom trace, red, VS=0.62). (C) Uncorrelated response of a scolopidial neuron to 1 Hz sinusoidal motion. (Top and bottom traces are the same as B. VS=0.14.) (D) A scolopidial neuron fires synchronous action potentials to a 25 Hz sinusoidal motion combined with its first harmonic 50 Hz (Top and bottom traces are the same as B.) (E) Comparison of the inverse of the ISI values of the first spikes within each stimulus oscillation with the stimulus frequency taken from the data in A (marks, means±s.d.; line, linear regression; slope=0.999; r^2=1). (F) Plot of the mean spike phase as a function of the stimulus frequency calculated from the data in A. The error bars represent s.d.

neuron, the average firing rate decreased from 130 to 100 Hz as stimulus frequency increased from 65 to 100 Hz.

Scolopidial neurons responded to 0.1–100 Hz sinusoidal motion in a phase-locked manner with little adaptation, even for stimuli exceeding 60 s. The maximum peak firing rates observed were around 200 Hz, occurring at the onset of stimulus. Fig. 4B illustrates an example of a partially phase-locked (VS=0.62) response to a 10 Hz sinusoidal stimulus. Although the spikes are partially phase locked in the first three stimulus cycles, their correlation with stimulus broke down over following cycles. When scolopidial neurons exhibited uncorrelated firing, we classified them as ‘independent’ (VS<0.5; Fig. 4C, VS=0.12). The neural responses usually increased with increasing stimulus amplitude. We could provide stimulus amplitudes up to 4 deg, beyond which our apparatus was limited by mechanical constraints of the passive flagellum–pedicel joint. As amplitude decreased, spiking frequency was lower and phase locking was weaker. Our stimulus range included both wingbeat (~22–27 Hz) and double wingbeat frequency (~44–54 Hz), at which antennae experience vibrational peaks in free flight (Sane et al., 2007). To investigate how both frequencies simultaneously shaped the scolopidial response, we presented composite stimuli made of two sinusoidal waves oscillating at these key frequencies. Scolopidial neurons showed strong phase locking to both frequencies, demonstrating the limited possibility of superposition of spiking responses (Fig. 4D). Here, the scolopidial neuron fired spikes at the lower reversal of the stimulus, possibly encoding the slope of upward motion or amplitude with spike rate. For frequency equal to or greater than 5 Hz, we computed the average value of interspike interval (ISI) times of the first spikes per stimulus oscillation period for data in Fig. 4A. The inverse of ISI means varied linearly with stimulus

The Journal of Experimental Biology (2014) doi:10.1242/jeb.101568

frequency (Fig. 4E, slope=0.999, r^2=1). We also plotted the mean spike phase as a function of stimulus frequency (Fig. 4F) for the data in Fig. 4A. The value of mean spike phase was roughly similar from 5–65 Hz, beyond which it increased with stimulus frequency.

Frequency-sweep stimuli

To rapidly estimate the frequency range in which scolopidia were most responsive to variations in stimulus frequency during intracellular recordings, we devised a constant-amplitude frequency-sweep stimulus in which the frequency increased linearly from 0 to 100 Hz over a period of 10 s (Fig. 5). The firing rate amplitude envelope of scolopidia phase locked with the stimulus at lower frequency (0–10 Hz, Fig. 5B–E, all cells). At higher frequencies (>20 Hz), scolopidia locked their firing rate with the linear increase in the stimulus frequency. Typically when cells responded linearly, they did so repeatedly, as exemplified by two repeats for each cell (Fig. 5B). However, when they did not encode stimulus frequency, they responded differently each time. Three neurons (Fig. 5B, 1, 3, 6; two repeats per cell) displayed linearly increasing GCFR at wingbeat frequency (approx. 25–30 Hz), six in twice wingbeat frequency range (Fig. 5, approximately 50–60 Hz, cells 2, 5, 7–9, 11), and eight neurons at three times wingbeat frequency (Fig. 5, approximately 75–90 Hz, cells 3–10).

The linear encoding scheme was independent of the sweep duration. Fig. 5C shows three trials in four neurons with varying time (7, 10 and 20 s sweeps; light, medium and dark blue traces, respectively) with the 7 and 20 s trials rescaled to 10 s. The linearly encoding segments remained mostly unchanged (Fig. 5C, neurons 6–9) when the stimulus duration was rescaled. We also investigated the effect of sweep stimuli played backward with frequencies decreasing from 100 to 0 Hz and variable durations (Fig. 5D, small box, 7, 10 and 20 s are represented by red, purple and orange traces, respectively). After rescaling the GCFR from the 7 and 20 s stimuli to 10 s and plotting the three trials in reverse time, their encoding

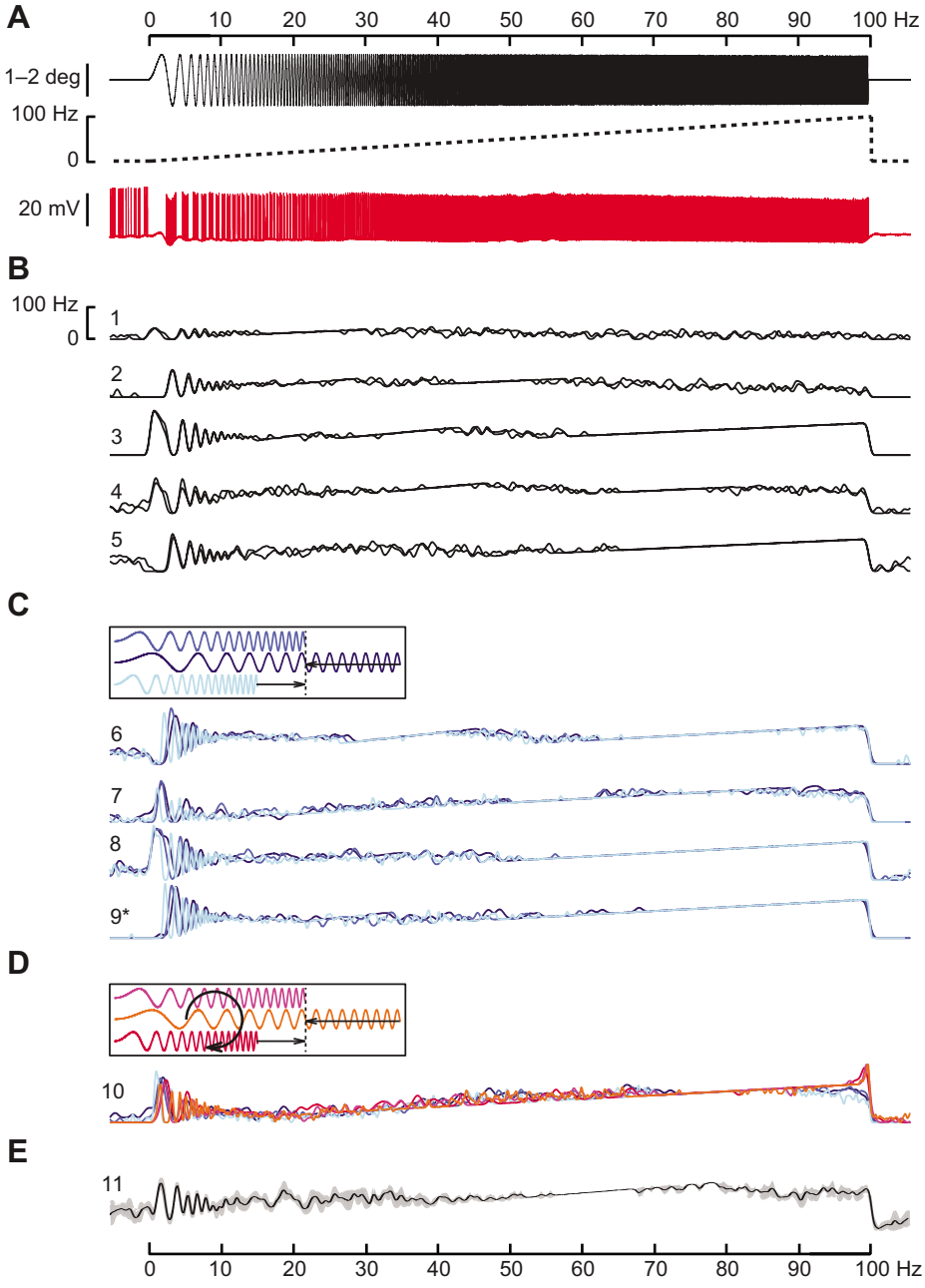

Fig. 5. Response of scolopidial neurons to frequency-sweep stimuli. (A) Top (black line): antennal frequency increases linearly from 0 to 100 Hz in 10 s. Middle (dotted black line): the linear increase in frequency. Bottom (red line): the membrane potential from one trial displaying the response of the scolopidial neuron to a frequency-sweep stimulus. (B) Numbers from 1 to 5 at the beginning of each plot mark a scolopidial neuron from a different animal. The black traces (two trials per cell) show the GCFR in response to the stimulus shown in A. (C) Scolopidial neurons 6–9, again, represent a different neuron in a different animal, and for each cell we show the GCFR from three trials in response to frequency-sweep stimuli from 0 to 100 Hz with three different time scales (light blue, 7 s; medium blue, 10 s; dark blue, 20 s), which have been normalized to the same *x*-axis, now representing frequency. Cell 9* (medium blue) is the GCFR representative of the action potentials of the red trace in A. The arrows indicate the rescaling of time. (D) Response from a single neuron (cell 10). The three blue traces are the same as those in C. The red traces represent three additional GCFRs in response to decreasing frequency-sweep stimuli from 100 to 0 Hz (red, 7 s; purple, 10 s; orange, 20 s) rescaled and plotted backward for visual comparison. The arrows indicate the forward and reverse rescaling of time. (E) GCFR from a previously published cell [number 11; same stimulus as A; fig. 2B from Sane et al. (Sane et al., 2007)]. The black trace with the shaded area represents the mean±s.d. of four trials.

The Journal of Experimental Biology (2014) doi:10.1242/jeb.101568

region remained linear around triple wingbeat frequency, similar to that responding to linear increase in frequency (Fig. 5D, blue traces similar to 5C, 75–85 Hz). Note the transient response at the stimulus onset occurring at the end of the trace when plotted backward (Fig. 5D, red, purple, orange lines). For comparison, we show in Fig. 5E (upper trace) the GCFR from another scolopidial neuron [fig. 2B from Sane et al. (Sane et al., 2007)] with a linear increase at double wingbeat frequency. The results in Fig. 5 remained unchanged for GCFRs with Gaussian windows of different width (supplementary material Fig. S1).

Phase locking and phase analysis of scolopidial neurons

To quantify the phase-locking response of scolopidial neurons for sinusoidal stimuli, we used two methods. At low stimulus frequencies of 0.1, 0.2, 1 and 5 Hz for which there was a high-frequency burst of spikes per cycle (Fig. 4A), the first spike of a new cycle was not always clearly separable from the previous burst making it an unreliable measure for phase locking. In such cases, we computed the cross-correlation coefficient between the stimulus and GCFRs to estimate phase locking of scolopidial neurons at these frequencies. All cells showed high cross-correlation coefficient (Fig. 6A, red) between the firing rate and stimulus. For frequencies of 5 Hz and higher, we used VS analyses to study the phase locking of a single spike to sinusoidal stimuli (Fig. 6A, black). If neurons fired at few spikes per cycle, we used the first spike to mark the phase for a specific stimulus cycle. For other spikes within a cycle (i.e. second and third within a burst), the computed VS did not yield significantly higher values than the first spikes. For a wide range of

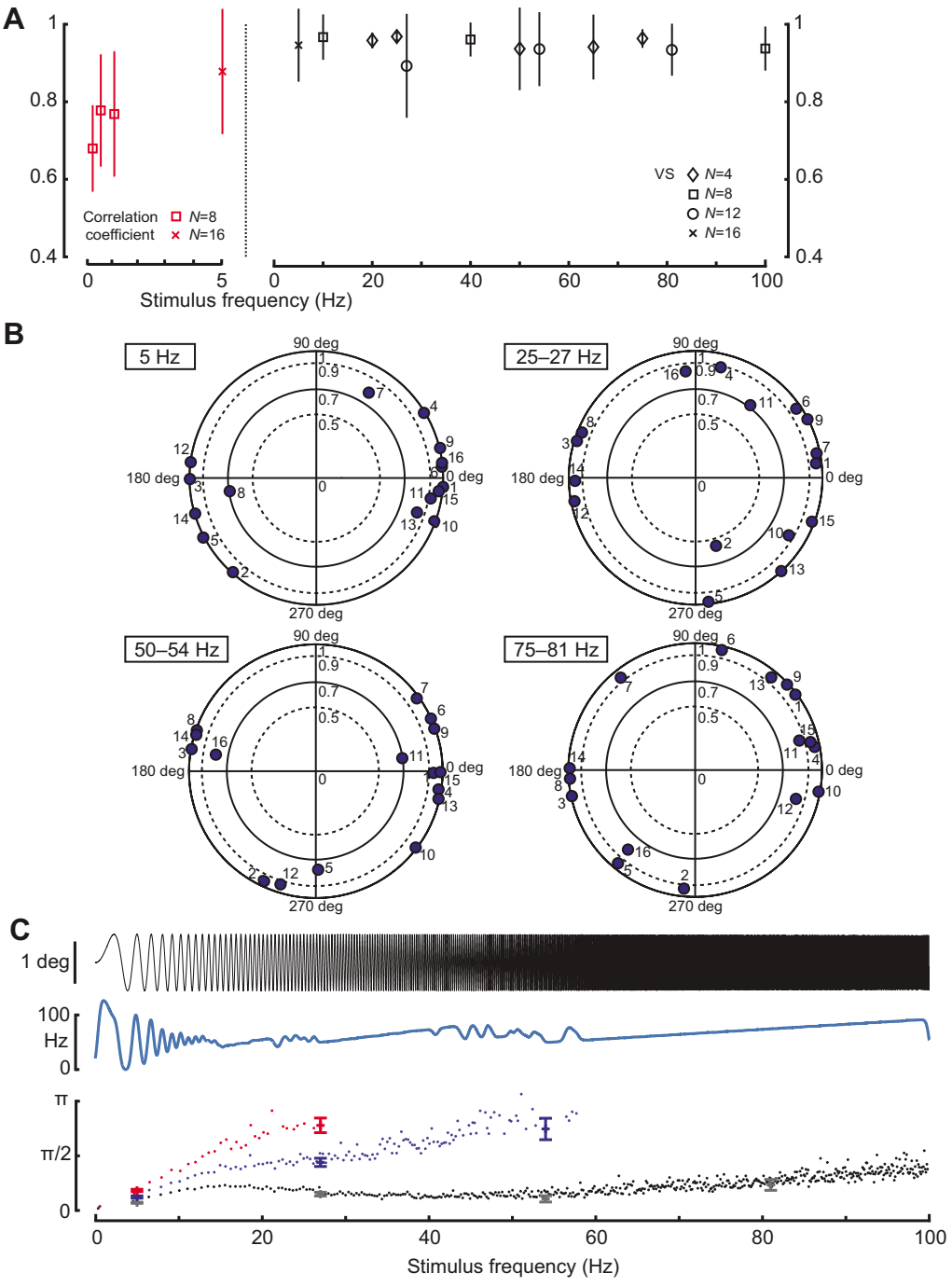

Fig. 6. Analysis of phase response of the scolopidial neurons. (A) Phase-locked responses of scolopidial neurons to sinusoidal frequency motion of 5 Hz and lower were quantified using correlation coefficients between the sinusoidal stimulus and the GCFR envelope (red; boxes, *N*=8; crosses, *N*=16). For frequencies of 5 Hz and greater, we used VS (black; diamonds, *N*=4 cells; boxes, *N*=8; circle, *N*=12; crosses, *N*=16 cells). For VS, values above 0.7 are considered phase locked ($P<0.001$, Rayleigh *Z*-test for deviation from circular uniformity). The symbols show the mean and the vertical lines represent the s.d. for N cells (each cell comes from a different animal). (B) Polar plots of the mean phase of the first spike within a cycle for the 16 cells shown in A (numbered 1 to 16). The distance from the center of the circles represents the VS ranging from 0 (center) to 1 (perimeter). Points above the inner solid circle (VS=0.7) are considered phase locked. Four frequency categories are represented (5, 25–27, 50–54 and 75–81 Hz) for the same cells. (C) The trace in the top panel (black) represents a sinusoidal sweep increasing linearly from 0 to 100 Hz in 10 s with its representative GCFR computed from one trial with a scolopidial neuron (corresponding to number 3 from Fig. 4B). The black, blue and red dots underneath represent, respectively, the phase of the first, second and third spikes computed for each cycle of the sweep. For comparison, we show in grey, blue and red the mean phase±s.d. for the first, second and third spikes, respectively, computed using sinusoidal motion.

The Journal of Experimental Biology (2014) doi:10.1242/jeb.101568

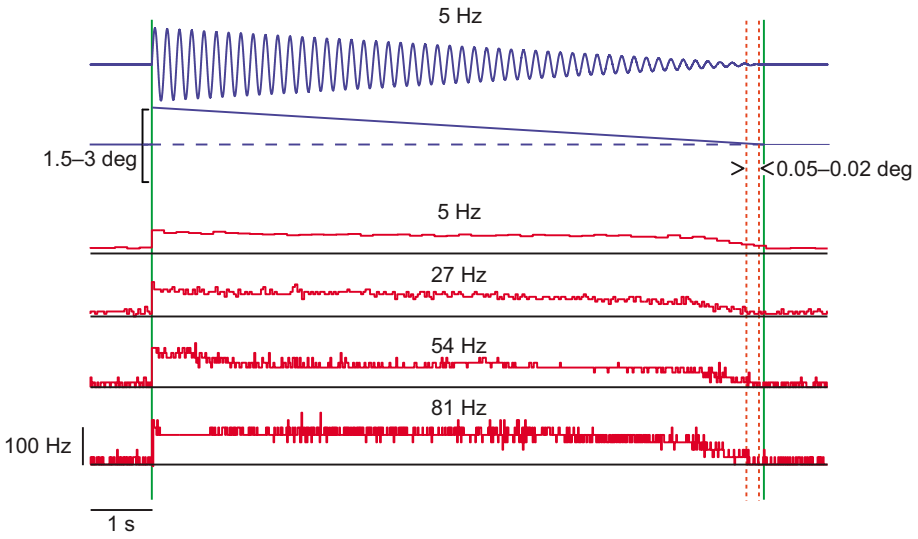

Fig. 7. Sensitivity of scolopidial neurons to varying amplitudes. Response of scolopidial neurons to amplitude-sweep stimuli at 5, 27, 54 and 81 Hz. The upper blue trace is one example of a 5 Hz sinusoidal amplitude-sweep stimulus and the lower blue trace represents the tapering of the amplitude versus time for all frequencies. The left and right vertical green lines show the onset and offset of the stimuli, respectively. The response of scolopidial neurons is calculated as the average firing rate for each cycle of the stimulus (red traces, *N*=4 cells from four individuals for all frequencies). The range between the red vertical dotted lines (0.05 to 0.02 deg) represents the minimum amplitudes, where the average firing rate per cycle is not differentiable from the spontaneous firing rate.

frequencies (5–100 Hz), all VS coefficients were greater than 0.7, indicating that scolopidial neurons were strongly phase locked with the stimuli.

To quantify the range of scolopidial neuronal sensitivity, we computed the phase response for the first spikes. We divided phase response into four categories (5, 25–27, 50–54, 75–81 Hz) representing low frequency, wingbeat frequency and two higher harmonics. In the polar plots of mean phase angle of the first spike with radius representing the VS (Fig. 6B), most points lay outside the smaller circle (Fig. 6B, solid line) representing a VS of 0.7 and were classified as phase locked. At low frequency (5 Hz), our sample of 16 neurons responded with a limited phase range, roughly 0 deg and 180 deg. This corresponded to part of the motion where antennal velocity is maximum, therefore it elicited the strongest neural responses. As stimulus frequency increased (Fig. 6B, 25–81 Hz), neurons responded to a wider distribution of phase values. The phase versus stimulus frequency relationship was irregular in most cells (supplementary material Fig. S2), but in a few cases it varied linearly with stimulus frequency, suggesting a temporal code. We did not observe a specific relationship between the phase of first, second and third spikes within a cycle when plotted against a wide range of frequencies (supplementary material Fig. S2, lower plot).

During frequency-sweep tests, the period between two cycles decreased non-linearly as frequency increased linearly. Using the sweep stimulus function, we computed an equivalent phase scale for each cycle within the sweep to determine the phase of subsequent spikes (Fig. 6C, first, second and third spikes represented by black, blue and red dots, respectively). We compared the phase with its standard deviation for the same cell for first, second and third spikes (Fig. 6C). Spikes occurring between 5 and 15 Hz were omitted for clarity. For this specific neuron, single, double and triple wingbeat frequencies were distinguished by the number of spikes (3, 2 and 1 respectively per period). The GCFR tends to encode the stimulus frequency linearly when the phases of second and third spikes show small variations from one cycle to the next.

Measurement of the sensitivity of scolopidial neurons to stimulus amplitude

To measure the sensitivity of scolopidial neurons to small displacements, we delivered amplitude-sweep stimuli at 5, 27, 54 and 81 Hz (Fig. 7). For each frequency, stimulus amplitude decreased linearly from a maximum of 3 deg to 0 deg in 10 s (Fig. 7, lower blue trace). Independent of stimulus frequency, scolopidial neurons were sensitive to amplitudes in a low range of 0.05–0.02 deg (between dotted red vertical lines). The average firing rate per cycle had the same mean and variance as the spontaneous firing rate. At stimulus onset, neurons showed a phaso-tonic response similar to step onset. The average firing rate per cycle remained unchanged when amplitude of antennal motion decreased from 3 deg to 0.5 deg. Thus for a large range of amplitudes, scolopidial neurons did not encode amplitude with firing rate. For amplitudes lower than 0.5 deg, the response sharply decreased. Although we cannot accurately model amplitude response of scolopidial neurons from this limited data set, their sensitivity to small amplitudes was evident.

DISCUSSION

In a previous study, we hypothesized that antennal mechanosensory feedback is crucial for flight control in the crepuscular hawk moth *M. sexta* based on behavioral and neurophysiology data (Sane et al., 2007). Specifically, we showed that this feedback was provided by individual scolopidia within the Johnson's organs, which detect passive flagellar vibrations. Attenuation of this feedback by removing the flagella of both antennae caused moths to lose control of their trajectories. Restoration of the feedback, by re-gluing the flagella, was sufficient to restore flight control. These data underscored the importance of scolopidial input for flight (Sane et al., 2007). Because scolopidia are the first neural elements to sense and encode relative movements between flagella and pedicel, it is important to determine how they encode mechanical stimuli that antennae experience during flight.

To our knowledge, the data described here, together with those reported in Sane et al. (Sane et al., 2007), are the first intracellular recordings from the antennal Johnston's organ and provide key insights into its encoding characteristics. The response latencies of the scolopidia to imposed mechanical stimuli are well under the duration of a wing stroke with strong phase locking to diverse frequencies of antennal motion. In many cases, scolopidial units fired at frequencies linearly proportional to the imposed antennal frequencies in the frequency domain of wingbeat frequency and its higher harmonics. The linear response range of each scolopidium is different, suggesting that the Johnston's organ is range fractionated. Scolopidial responses are exquisitely sensitive to antennal deflections as low as 0.02 deg with some indication of directional sensitivity (supplementary material Fig. S3). Finally, all scolopidia arborize within the AMMC. Thus, the AMMC in the deutocerebrum

is likely to be a region of primary importance for antennal motion integration. Inputs from diverse modalities, including vision and Böhm's bristles, also arborize in the AMMC (Krishnan et al., 2012; Krishnan and Sane, 2014).

Range fractionation of the scolopidia in Johnston's organs

Recent work shows that the scolopidial units of Johnston's organs sub-serve different functions, including gravity, auditory and airflow sensing (Kamikouchi et al., 2009; Yorozu et al., 2009), most probably resulting from different tuning properties of these neurons. Specifically, scolopidia with low-pass tuning characteristics are likely to serve the functions of gravity or airflow sensing, whereas high-pass tuned scolopidia serve the function of audition or vibration sensing. Thus, different tuning properties of individual scolopidia may be the basis of the multi-functionality of the Johnston's organs.

A large fraction of scolopidial cells tightly phase locked (VS>0.9) to sinusoidal motions within the 0–100 Hz frequency range (Table 1; Fig. 6A) and had similar morphology and patterns of arborization. This contrasts with systems in which each scolopidium contains distinct neuron types with different firing responses to sustained mechanical or electrical stimuli (spider slit sensilla; Seyfarth and French, 1994; Gingl et al., 2006). In these experiments, scolopidia neurons were tuned to sinusoidal motion and frequency-sweep stimuli in the 0–100 Hz range (Table 1; Figs 4–6). Within this frequency range, neurons robustly responded to small oscillation flagellar amplitudes (<0.05 deg, Fig. 7). This sensitivity explains artifacts in step stimulus experiments, because scolopidia responded to very small ringing motions of the servomotor after onset of the step (Fig. 3B, small oscillations in blue trace). Interestingly, the firing frequency in some scolopidial neurons linearly increased in response to frequency-sweep stimuli in a range encompassing the wingbeat frequency and its two higher harmonics (respectively 22–27 Hz, 44–54 Hz and 66–91 Hz). The latter response may be relevant for flight because moth antennae experience significant forces at wingbeat frequency and twice wingbeat frequency during active flight (Sane et al., 2007).

In most experiments, we could move the antennae only in one dimension at a time owing to the limitations of the servomotor system. To overcome this constraint, we conducted a few experiments with a smaller servo motor allowing us to rotate the stimulus by 90 deg and study the response of the neuron along two axes of motion spanning four orientation quadrants. These experiments indicated that the units of the Johnston's organ were directionally sensitive, with distinct response characteristics in different directions (supplementary material Fig. S3A,B). Although we tried to constrain the stimulus to a single axis, we could not rule out some small residual motion along other axes at higher frequencies (>50 Hz). The high sensitivity of scolopidia to small amplitude motions makes the influence of such artifacts difficult to rule out. These caveats must be considered when discussing the main implications of these results.

Latency of scolopidial responses

The multiple repeats of step stimuli in several scolopidial neurons and moths allowed us to estimate the latency with which scolopidial stimulation is transmitted to the AMMC (Fig. 3). The recording site was typically near the mid-point of the total distance between sensory neurons and their arbor within the AMMC. Assuming that the times of opening and closing of ion channels near the soma are negligible, the duration of transmission of the sensory stimulus to AMMC is, by the most liberal estimate, twice the value at the recording site. From Fig. 3B, this value lies between 2 and 3 ms, depending on whether we choose the initial rise or peak of the response to determine latency. From these considerations, latency at the AMMC following scolopidial stimulation is 4–6 ms, which is likely to be an overestimate because the transduction of mechanical to electrical signals is a substantial fraction of the time between scolopidial stimulation and arrival of spikes at the recording site.

The value of 4–6 ms is smaller by an order of magnitude than the typical wing stroke period (40 ms) and also much faster than lobula plate visual neuron latency in dark-adapted moths (>80 ms; Theobald et al., 2010). Because such rapid responses are necessary for proper stabilization of flight on a stroke-to-stroke basis (Hedrick and Daniel, 2006), antennal mechanosensory feedback complements the visual system for flight control. Any disruption or reduction of this input may cause specific flight-related problems, especially under conditions of insufficient or slow visual feedback. This is observed, for instance, in *M. sexta* individuals with ablated flagella flying under low light conditions, which are unable to control flight (Sane et al., 2007).

Morphological similarity of scolopidial neurons

The filled scolopidial neurons (N=43 cells, 23 individuals) shared many common features of morphology and location. Because we fixed the preparation to eliminate movement of all joints except the pedicel–flagellar joint, our experiments were inherently biased against identification of other mechanosensory neurons (e.g. ~500 Böhm's bristle neurons), which probably remained quiescent during the experiment. The axons of olfactory neurons are comparatively smaller in diameter, making it less likely to access these neurons via intracellular recordings as compared with mechanosensory axons of larger diameter.

Each scolopidium typically consists of four cell types arranged in a linear manner. These include one to four bipolar neurons with dendrites terminating in a ciliary structure, a scolopale cell enveloping the sensory cell dendrite, one or more attachment cells associated with the distal region of scolopale cell and one or more glial cells surrounding the neuronal soma (Yack, 2004; Field and Matheson, 1998). In *M. sexta*, the scolopidial units of antennal Johnston's organ contain a single bipolar neuron (Vande Berg, 1971). It is not clear whether these neurons are mononematic (an attachment cell with a stretching mechanotransduction mechanism) or amphinematic (with a cap transducing the motion by bending the ciliary structure). However, our observations of the Johnston's organ anatomy (Fig. 2) were consistent with those of Vande Berg (Vande Berg, 1971). From a cursory inspection, their cell body morphologies were similar to each other, but different from the cockroach Johnston's organ in which each scolopidial unit contains two neurons with different morphologies with one type displaying a swollen part of its ciliary terminal (Ikeda et al., 2004). At higher magnification (×600), we observed the extension of the ciliary tip with its ciliary dilation and possible attachment to the first annulus of flagellum (Fig. 2C). Because this ciliary extension provides a direct connection between mechanosensory scolopidium in the pedicel and the base of flagellum, it is the first transduction element to sense any deformation in the pedicel–flagellum joint. This biomechanical arrangement could function as a transducer of flagellar deflection comparable to an axial tendon placed upon the cilium with presumably mechanosensitive ion channels responding to that tension. Although the close apposition of neurons (Fig. 2C) suggests a heterodynal structure with two (or more) neurons per scolopidium, autofluorescence from tissues surrounding the scolopidium (Fig. 2Ci) displayed a single neuron per unit, suggesting a monodynal structure with a single neuron per scolopidium.

The projections of all scolopidial neurons terminated within the AMMC. We observed some differences among imaged neurons in their patterns of arborization in the AMMC. Some had concentric branching, whereas others displayed elongated branches extending towards subesophageal ganglia (Fig. 3B). Böhm's bristle afferents also arborize in the AMMC forming direct connections with antennal motoneurons (Krishnan et al., 2012). However, it remains unclear how these two mechanosensory inputs are integrated by downstream neurons.

Encoding schemes for scolopidial neurons

When the antenna was stationary, scolopidial neurons fired with a low spontaneous rate (e.g. Fig. 3). During experiments, higher spontaneous firing rates were sometimes observed when the flagellum was presumably under tension due to coupling between the antennal apparatus and stimulating device. Axial pull on the whole flagellum typically generated a strong response and high spontaneous firing behavior. The spontaneous rate could be sometimes adjusted with DC offset, especially because scolopidial neurons showed little adaptation. Some neurons responded exclusively to onset, whereas others responded to both onset and offset of step stimuli, probably dependent on the specific location of scolopidial soma relative to imposed flagellar motion. Thus, maximum strain on cilium could originate from the sharp motion of the step, independent of motion direction.

Whether the underlying encoding strategy is rate- or timing-based depends largely on how the signals are integrated by post-synaptic neurons. The post-synaptic cells in AMMC could use different strategies to integrate spikes from strongly phase-locked scolopidia in response to stimuli within the 0.2–100 Hz frequency range (Figs 4, 5). For example, at stimuli of lower frequencies (<5 Hz), the firing rate amplitude modulations of scolopidial neurons correlated with stimulus oscillations (first row, Fig. 4; also Fig. 6A, red). Thus, post-synaptic cells with large integration time constants could track the envelope of firing rate amplitudes to track the antennal motion. At stimulus frequencies greater than 10 Hz, however, the firing rate amplitude envelope flattens out and does not oscillate at stimulus frequency. The scolopidial responses showed a linear increase in GCFR tracking with an increase in stimulus sweep frequency (Fig. 5). In such cases, post-synaptic cells may be rate-coded. Alternatively, post-synaptic neurons with shorter integration time constants could take advantage of the precise spike timing to track the frequency of flagellar motion. At frequencies lower than 60 Hz, scolopidial neurons often fired more than one spike per period of oscillation (>50 spikes per period for very low frequencies), which may lead to ambiguity for a temporal coding scheme.

The above strategies could work in concert to integrate flagellar movements with great reliability. For example, scolopidia tend to fire around 2–3 spikes at wingbeat frequency, 1–2 at double wingbeat frequency and 1 spike at higher frequencies while tracking the stimulus with a linear increase in their firing rate (Fig. 6C). Yet, four spikes at 25 Hz, two at 50 Hz and one at 100 Hz produce the same firing rate preventing downstream neurons from measuring proper stimulus frequency. Here, tracking the timing of the first spike per oscillation could provide correct stimulus frequency.

Phase sensitivity of scolopidial neurons

For the cell in Fig. 4A, the inverse of ISI varied linearly with stimulus frequency with very low standard deviation (Fig. 4E), indicating a rate-encoded strategy. In this neuron however, the mean spike phase remained roughly unchanged with high variability for frequencies below 65 Hz, beyond which spike phase increased approximately linearly with stimulus frequency (Fig. 4F). Interestingly, 65–70 Hz is also the stimulus frequency beyond which neurons fire only one spike per stimulus cycle (Fig. 4A). Thus, when stimulus frequency exceeds the capacity of a sensory neuron for rate encoding, the neuron may switch to phase encoding. Similarly, for the neuron in Fig. 6C, the first spike phase remains roughly constant below 60 Hz, but increases approximately linearly with stimulus frequency above 60 Hz. Typically, the phase response of scolopidia to sinusoidal antennal motions has a high VS (Fig. 6A) but their mean phase versus stimulus frequency varies greatly from cell-to-cell (supplementary material Fig. S2). In some cases, mean phase varies monotonically with stimulus frequency (e.g. cells 12, 16; supplementary material Fig. S2, top panel), whereas in others, the relationship between mean phase and stimulus frequency is ambiguous. Consequently, describing the temporal encoding strategy requires a more targeted approach (e.g. white noise analysis; Fox et al., 2010). Such an approach can help reconstruct linear or non-linear models of rate or phase encoding, which is not possible with the simpler stimulus protocols.

Relevance of scolopidial encoding properties for flight control

Mechanosensory antennal inputs are crucial for flight control in *M. sexta* and other moths. During flight, their antennae undergo small amplitude oscillations at wingbeat frequency. These vibrations are sensed by scolopidia of the Johnston's organ, which are extremely sensitive both to small flagellar displacement and the direction of antennal motion. Owing to their sensitivity in specific frequency bands, they can encode antennal motion arising from diverse causes (Kamikouchi et al., 2009; Yorozu et al., 2009). At low frequency stimulation, Johnston's organs may serve an air-flow sensing function, perhaps in concert with inputs from Böhm's bristles (Heran, 1957; Gewecke, 1974). On the other hand, their high sensitivity to small amplitude, high frequency oscillations indicates their ability to precisely transduce small vibrations, including the frequency and amplitude of antennal motion due to Coriolis torques (Sane et al., 2007). Further studies are required to understand function-specific spatial distribution of scolopidia within Johnston's organ and their downstream targets in the nervous system.

In summary, our study presents direct recordings from single neurons in the Johnston's organs and showcases their range and exquisite sensitivity of their response to small amplitude, high frequency motion of the flagellum.

MATERIALS AND METHODS

Anatomy

The *M. sexta* antenna has three major segments: a proximal scape connected to pedicel and distal multi-annular flagellum (Fig. 1Ai,ii) is actively controlled by at least five extrinsic muscles and moves within a ball-and-socket joint in the head capsule (Kloppenburg et al., 1997). The pedicel is actuated by at least four intrinsic muscles within the scape. In contrast to the scape and pedicel, flagellar movements are entirely passive due to lack of muscles. The flagellum consists of olfactory sensillae and some mechanosensory bristles. The scape and pedicel contain two types of mechanosensors. One type, called Böhm's bristles, are organized as discrete fields on the scape and pedicel surface. Another type, called Johnston's organ, is a circumferential ring of scolopidia within the pedicel with attachments to the first flagellar annulus. In *M. sexta*, the Johnston's organ consists of ~650 scolopidia (Vande Berg, 1971), which encode minute deflections of the passive flagellar–pedicel joint due to flagellar motion. Unlike other insects, a connective chordotonal organ along the central pedicel axis has not been observed in *M. sexta*, nor is the presence of campaniform sensillae in antennae reported (Field and Matheson, 1998).

The Journal of Experimental Biology (2014) doi:10.1242/jeb.101568

The antennal sensory and motor apparatus is connected to the brain via a forked antennal nerve. All antennal mechanosensory projections and antennal motor neuron cell bodies are located in the deutocerebrum in a region called the AMMC (Kloppenburg et al., 1997).

Preparation

The experiments reported here were performed on 1–3 day post-eclosion adult male and female *M. sexta* (Lepidoptera: Sphingidae) from a colony maintained at the University of Washington. Before dissection, animals were cold-anesthetized at 4°C for 1–2 hours. Scales were removed from upper thorax, antennal base and head capsule to enable dissection and application of wax to stabilize the neck during intracellular recordings. Anesthetized moths were mounted dorsal side-up in a plastic tube and secured with a mixture of beeswax-rosin, leaving exposed the head, antennae and front of the thorax (Fig. 1B). This preparation restricted head motions and spurious mechanical vibrations thus enabling stable intracellular recordings. A small copper rod attached to the front of tube was waxed to the anterior–ventral aspect of the head and proboscis and served as a head restraint. The tube was positioned at a 30 deg angle on a vibration isolation table (TMC). To gain access to the brain and antennal nerve, we made a rectangular window by removing the dorsal head cuticle. The esophagus and some extrinsic antennal muscles were also dissected in some cases to gain access to the antennal nerve.

Stimulus generation

To ensure that imposed antennal motion directly stimulated the passive flagellar–pedicel joint, we immobilized the active scape–pedicel joint with a beeswax–rosin mixture. Active joints were held fixed at inter-antennal angles of approximately 145 deg, similar to freely flying moths. Antennal bending during mechanical stimulation was minimized by inserting the flagellum into a glass micropipette [inner (outer) diameters of 1.1 mm (1.7 mm) for male flagella and 0.8 mm (1.35 mm) for female flagella] and affixing it with wax leaving only a few annuli of the flagellum exposed at the base. The enclosed antenna was attached to a custom-made hinge and a thin tungsten wire with a hook to enable free rotation. Thus, the applied stimulus could be directly transmitted to the antennal base. The tungsten wire was held by a short glass capillary tube [inner (outer) diameters of 1.1 mm (1.7 mm)] lubricated with Vaseline® and controlled by a micromanipulator to serve as a guide, keeping the motion linear while holding the flagellum. The other end of the tungsten wire was glued via a small bearing (3 mm, Small Parts Inc., Logansport, IN, USA) to a voltage-controlled servomotor lever system (300B series, Aurora Scientific Inc., Dublin, Ireland) enabling us to deliver pre-programmed mechanical stimuli to the pedicel–flagellum joint. In each trial, the motion was linear but the orientation varied between animals. The maximum amplitude deflection was constrained by the pedicellar–flagellar joint but never exceeded 5 deg (to avoid cracking the beeswax–rosin seal). Typically, the amplitude of antennal motion was kept between 2–3 deg, corresponding to 0.75–1.25 mm of quasi-linear displacement of the flagellar tip (Fig. 1B).

In some experiments, the glass micropipette enclosing the antenna was attached to a galvanometric mini-CT shaft controlled by a 6200H servo driver (Cambridge Technology, Lexington, MA, USA) tuned to inertial loads of the micropipette. The flagellum was shortened, leaving a proximal part of ~20 annuli. Cutting the flagellum did not affect the Johnston's organ response. The remaining flagellar stump was inserted directly inside the glass capillary and the motor was aligned at a proper angle relative to the scape and pedicel. Because the motor rotated through less than 3 deg, flagellar motion was quasi-linear. Moreover, although unidirectional motion was applied during each recording trial, the motor could be rotated between trials to mimic stimulations in two spherical axes of antennal motion.

The servo motor-lever system interfaced with a data acquisition card (PCI MIO 16E4 DAQ, National Instruments, Austin, TX, USA) and was controlled by a custom MATLAB program (The MathWorks, Natick, MA, USA). This interface provided an analog output to the lever system, with simultaneous acquisition of electrophysiological data. We moved the antenna following pre-programmed sinusoidal and step motions, as well as frequency and amplitude sweeps. We used two methods to ensure fidelity of the actual versus intended motion through the hinge system. First, we recorded the analog signal from the servomotor at 10 kHz during intracellular recording sessions (see below) which accurately reported the instantaneous lever position. Second, we measured and calibrated motion of the flagellar–pedicel joint using a custom photodiode and phototransistor system (Fig. 1C). Using this setup, we could provide precise mechanical stimuli to the pedicel–flagellar joint within the limitations of the coupling system and the antennal apparatus.

Electrophysiology and neuroanatomy

We recorded from the axons of 96 individual scolopidial neurons in the antennal nerve. A flat hook, fabricated by bending a syringe needle tip (gauge 33), mechanically stabilized the antennal nerve during intracellular exploration and penetration, and also served as a ground electrode (Fig. 1B). The exposed nervous tissue was bathed in the moth's own hemolymph and supplemented with additional *Manduca* physiological saline solution [150 mmol l^{-1} NaCl, 3 mmol l^{-1} $CaCl_2$, 3 mmol l^{-1} KCl, 10 mmol l^{-1} N-tris(hydroxymethyl)methyl-2-aminoethane sulfonic acid buffer and 25 mmol l^{-1} sucrose, pH 6.5–7.5; Lei et al., 2004] as needed. To record from and stain afferent neurons, we used medium-walled quartz micropipettes (Sutter Instruments, Novato, CA, USA; resistance=100–150 MΩ in saline) filled with 5% Lucifer Yellow and LiCl or Alexa Fluor and KCl. When required, the neurons were held slightly hyperpolarized to obtain stable recordings. Intracellular signals were amplified 10-fold with an intracellular amplifier (A-M systems, Sequim, WA, USA) and 60 Hz noise was filtered out with a Hum Bug (Quest Scientific, North Vancouver, BC, Canada). With these methods, we obtained stable intracellular records for durations of 10–45 min. Neurons were stained iontophoretically by injecting the dye using constant negative 2.0 nA current for 5–30 min.

After each experiment, the brain was dissected in *Manduca* saline, fixed in formalin (10% neutral buffered, Sigma) for 1 h and dehydrated through an ethanol series. After clearing in methyl salicylate, we imaged the brain using a laser-scanning confocal microscope (Bio-Rad MRC 2000, Hercules, CA, USA). The thickness of the optical image sections ranged from 0.15–10 µm. We used ImageJ (National Institutes of Health, Bethesda, MD, USA) software to obtain planar projections of each section.

Identification of sensory neurons

We applied 1–3 Hz mechanical sinusoidal motion stimuli to the flagellar–pedicel joint while probing the antennal nerve for scolopidial axons. Although a vast majority of axons passing through antennal nerves are olfactory (>262,000; Sanes and Hildebrand, 1976), these axons were typically small (<1 µm diameter) and difficult to access for intracellular recordings. In contrast, axons from mechanosensory neurons, although far fewer (<1500) in number were larger in diameter, allowing both access and hold. Thus we could perform repeated, reproducible and stable intracellular recordings from scolopidia. Typically, we began a recording session after observing stimulus-correlated spiking at resting potentials between −40 and −60 mV and spike amplitudes >10 mV.

Stimulus protocols

Most protocols consisted of: (1) repeated step stimuli of varying duration (5–30 s) to generate a PSTH, (2) sinusoidal stimuli consisting of 10, 5 s sub-trials at 0.2, 1, 5, 25, 50, 65 and 100 Hz, (3) constant-amplitude sinusoidal sweeps increasing linearly in frequency from 0.1 to 100 Hz in 5, 10 or 20 s (frequency-sweep, Table 1) and, (4) constant-frequency sinusoidal sweeps of 5, 27, 54 and 81 Hz decreasing linearly in amplitude from 1.5–3 deg to 0 deg in 10 s (amplitude-sweep).

Estimation of response latency

We estimated the approximate time required for the relay of mechanical stimulus to the AMMC using the above measurements. Because most recordings from scolopidial axons were performed approximately 0.4–0.7 mm from the soma near the mid-point of the antennal nerve (Fig. 2A), the distance between the scolopidial soma and its terminus in the AMMC was approximately 0.8–1.4 mm. The time between stimulation and onset of spiking activity at the recording site may thus be doubled to estimate the total latency of relay from the periphery to the AMMC. We

could not estimate axonal conduction velocity from this because the opening and closing times of ion channels following mechanical stimulation of antennae may be a substantial component of total latency, which was not measured.

Analysis of phase locking

To quantify how precisely a neuron locks its phase of spiking with the mechanical stimulus, we used two types of characterizations. For stimulus frequencies of 5 Hz and greater, we used the VS equation (Goldberg and Brown, 1969; Batschelet, 1981) to determine the phase of the first spike within a burst for each cycle or a single spike generally produced at higher frequencies.

$$\mathrm{VS}=\left(\frac{1}{n}\right)\sqrt{\left(\sum_{t=1}^{n}\cos\left(\frac{2\pi\left(t_\mathrm{i}-t_\mathrm{peak}\right)}{T}\right)\right)^2+\left(\sum_{t=1}^{n}\sin\left(\frac{2\pi\left(t_\mathrm{i}-t_\mathrm{peak}\right)}{T}\right)\right)^2}, \quad (1)$$

where n is the number of spikes, and

$$\left(\frac{2\pi\left(t_\mathrm{i}-t_\mathrm{peak}\right)}{T}\right) \quad (2)$$

is the phase of i$^{\mathrm{th}}$ spike (t_i) relative to the preceding stimulus peak (t_peak) divided by period (T) of the stimulus cycle. We used Rayleigh's Z-test to determine whether VS was sufficiently high for phase locking. In all instances, we rejected the null hypothesis (the phases are randomly distributed) with $P<0.001$. The computed values were $0<P<8.23\times10^{-6}$ and $10.42<Z\text{-statistic}<488.97$. Here, we describe scolopidial neurons with VS>0.7 as phase locked to the stimulus, between 0.5 and 0.7 as partially phase locked and less than 0.5 as independent.

For frequency stimuli of 5 Hz and lower, very long bursts of spikes (>10) per stimulus period meant that the VS analysis method using the first spike was not reliable. For these cases, we computed cross-correlation coefficients between the sinusoidal stimulus and GCFR (window width=500 ms, s.d.=31.6 ms) using the xcorr function in MATLAB.

Acknowledgements

We thank Binh Nguyen for moth breeding and members of Daniel and Sane laboratories for critical comments on the manuscript. We also wish to gratefully thank an anonymous referee for constructive feedback.

Competing interests

The authors declare no competing financial interests.

Author contributions

A.D., T.L.D. and S.P.S designed the experiments. A.D. performed the experiments and analyzed the data. A.D. and S.P.S interpreted the data and prepared the manuscript. A.D., T.L.D. and S.P.S revised the manuscript.

Funding

This work was funded by Air Force Office of Scientific Research; Office of Naval Research; Joan and Richard Komen Endowed Chair to T.L.D.; and the National Science Foundation Interdisciplinary Informatics Grant and Ramanujan Fellowship to S.P.S.

Supplementary material

Supplementary material available online at
http://jeb.biologists.org/lookup/suppl/doi:10.1242/jeb.101568/-/DC1

References

Batschelet, E. (1981), *Circular Statistics in Biology*. New York, NY: Academic Press.
Budick, S. A., Reiser, M. B. and Dickinson, M. H. (2007). The role of visual and mechanosensory cues in structuring forward flight in *Drosophila melanogaster*. *J. Exp. Biol.* **210**, 4092-4103.
Fayyazuddin, A., Dickinson, M. H. (1996). Haltere afferents provide direct, electronic input to a steering motor neuron in the blowfly, *Caliphora*. *J. Neurosci.* 16, 5225-5232.
Field, L. H. and Matheson, T. (1998). Chordotonbal organ of insects. *Adv. In Insect Phys.* **27**, 1-56; C1-C2, 57-228.
Fox, J. L. and Daniel, T. L. (2008). A neural basis for gyroscopic force measurement in the halteres of *Holorusia*. *J. Comp. Physiol. A* **194**, 887-897.
Fox, J. L., Fairhall, A. L. and Daniel, T. L. (2010). Encoding properties of halteres enable motion feature detection in a biological gyroscope. *Proc. Natl. Acad. Sci. USA* **107**, 3840-3845.
Frye, M. A., Dickinson, M. H. (2004). Closing the loop between neurobiology and flight behavior in *Drosophila*. *Curr Op. Neurob.* **14**, 729-736.
Gewecke, M. (1974). The antennae of insects as air-current sense organs and their relationship to the control of flight. In *Experimental Analysis of Insect Behaviour* (ed. L. B. Browne), pp. 100-113. Berlin: Springer.
Gewecke, M. and Niehaus, M. (1981a). Flight and flight control by the antennae in the small tortoiseshell (*Aglais urticae* L., Lepidoptera). 1. Flight balance experiments. *J. Comp. Physiol.* **145**, 249-256.
Gewecke, M. and Niehaus, M. (1981b). Flight and flight control by the antennae in the small tortoishell (*Aglais urticae* L., Lepidoptera). 2. Flight mill and free flight experiments. *J. Comp. Physiol.* **145**, 249-256.
Gingl, E., Burger, A.-M. and Barth, F. G. (2006). Intracellular recording from a spider vibration receptor. *J. Comp. Physiol. A* **192**, 551-558.
Goldberg, J. and Brown, P. (1969). Response of bunaural neurons of dog superior olivary complex to dichotic tonal stimuli: some physiological complex to dichotonic tonal stimuli: some physiological mechanisms of sound localization. *J. Neurophysiol.* **32**, 613-636.
Hardie, R. C. and Raghu, P. (2001). Visual transduction in *Drosophila*. *Nature* **413**, 186-193.
Hedrick, T. L. and Daniel, T. L. (2006). Flight control in the hawkmoth *Manduca sexta*: the inverse problem of hovering. *J. Exp. Biol.* **209**, 3114-3130.
Hengstenberg, R. (1988). Mechanosensory control of compensatory head roll during flight in the blowfly *Calliphora erythrocephala* Meig. *J. Comp. Physiol. A* **163**, 151-165.
Heran, H. (1957). Die bienenantenne als messorgan der flugeigengeschwindigkeit. *Naturwissenschaften* **44**, 475.
Hinterwirth, A. J. and Daniel, T. L. (2010). Antennae in the hawkmoth *Manduca sexta* (Lepidoptera, Sphingidae) mediate abdominal flexion in response to mechanical stimuli. *J. Comp. Physiol. A* **196**, 947-956.
Hinterwirth, A. J., Medina, B., Lockey, J., Otten, D., Voldman, J., Lang, J. H., Hildebrand, J. G. and Daniel, T. L. (2012). Wireless stimulation of antennal muscles in freely flying hawkmoths leads to flight path changes. *PLoS ONE* **7**, e52725.
Ikeda, S., Toh, Y., Okamura, J. Y. and Okada, J. (2004). Intracellular responses of antennal chordotonal sensilla of the American cockroach. *Zoolog. Sci.* **21**, 375-383.
Kamikouchi, A., Shimada, T. and Ito, K. (2006). Comprehensive classification of the auditory sensory projections in the brain of the fruit fly *Drosophila melanogaster*. *J. Comp. Neurol.* **499**, 317-356.
Kamikouchi, A., Inagaki, H. K., Effertz, T., Hendrich, O., Fiala, A., Göpfert, M. C. and Ito, K. (2009). The neural basis of *Drosophila* gravity-sensing and hearing. *Nature* **458**, 165-171.
Kloppenburg, P., Camazine, S. M., Jun Sun, X., Randolph, P., Hildebrand, J. G. (1997). Organization of antennal motor system in the sphinx moth *Manduca sexta*. *Cell Tissue Res.* **287**, 425-433.
Krishnan, A. and Sane, S. P. (2014). Visual feedback influences antennal positioning in flying hawk moths. *J. Exp. Biol.* **217**, 908-917.
Krishnan, A., Prabhakar, S., Sudarsan, S. and Sane, S. P. (2012). The neural mechanisms of antennal positioning in flying moths. *J. Exp. Biol.* **215**, 3096-3105.
Lei, H., Christensen, T. A. and Hildebrand, J. G. (2004). Spatial and temporal organization of ensemble representations for different odor classes in the moth antennal lobe. *J. Neurosci.* **24**, 11108-11119.
Mamiya, A., Straw, A. D., Tómasson, E. and Dickinson, M. H. (2011). Active and passive antennal movements during visually guided steering in flying *Drosophila*. *J. Neurosci.* **31**, 6900-6914.
Nalbach, G. (1993). The halteres of the blowfly *Calliphora*. *J. Comp. Physiol. A* **173**, 293-300.
Niehaus, M. and Gewecke, M. (1978). The antennal movement apparatus in the small tortoiseshell (*Aglais urticae* L., Lepidoptera). *Zoomorphologie* **91**, 19-36.
Pringle, J. W. S. (1948). The gyroscopic mechanism of the halters of Dipetera. *Philos. Trans. R. Soc. B* **233**, 347-384.
Sane, S. P., Dieudonné, A., Willis, M. A. and Daniel, T. L. (2007). Antennal mechanosensors mediate flight control in moths. *Science* **315**, 863-866.
Sanes, J. R. and Hildebrand, J. G. (1976). Structure and development of antennae in a moth, *Manduca sexta*. *Dev. Biol.* **51**, 282-299.
Seyfarth, E.-A. and French, A. S. (1994). Intracellular characterization of identified sensory cells in a new spider mechanoreceptor preparation. *J. Neurophysiol.* **71**, 1422-1427.
Theobald, J. C., Warrant, E. J. and O'Carroll, D. C. (2010). Wide-field motion tuning in nocturnal hawkmoths. *Proc. Biol. Sci.* **277**, 853-860.
Vande Berg, J. S. (1971). Fine structural studies of Johnston's organ in the tobacco hornworm moth, *Manduca sexta* (Johannson). *J. Morphol.* **133**, 439-455.
Warrant, E. J. (2006). Invertebrate vision in dim light. In *Invertebrate Vision* (ed. E. J. Warrant and D.-E. Nilsson), pp. 83-126. Cambridge: Cambridge University Press.
Yack, J. E. (2004). The structure and function of auditory chordotonal organs in insects. *Microsc. Res. Tech.* **63**, 315-337.
Yorozu, S., Wong, A., Fischer, B. J., Dankert, H., Kernan, M. J., Kamikouchi, A., Ito, K. and Anderson, D. J. (2009). Distinct sensory representations of wind and near-field sound in the *Drosophila* brain. *Nature* **458**, 201-205.